Nucleon binding energy and transverse momentum imbalance in neutrino-nucleus reactions

T. Cai,[1] X.-G. Lu,[2] L.A. Harewood,[3] C. Wret,[1] F. Akbar,[4] D.A. Andrade,[5] M. V. Ascencio,[6] L. Bellantoni,[7] A. Bercellie,[1] M. Betancourt,[7] A. Bodek,[1] J. L. Bonilla,[5] A. Bravar,[8] H. Budd,[1] G. Caceres,[9] M.F. Carneiro,[10] D. Coplowe,[2] H. da Motta,[9] Zubair Ahmad Dar,[4] G.A. Díaz,[1,6] J. Felix,[5] L. Fields,[7,11] A. Filkins,[12] R. Fine,[1] A.M. Gago,[6] H. Gallagher,[13] A. Ghosh,[14,9] R. Gran,[3] D.A. Harris,[7] S. Henry,[1] S. Jena,[15] D.Jena,[7] J. Kleykamp,[1] M. Kordosky,[12] D. Last,[16] T. Le,[13,17] A. Lozano,[9] E. Maher,[18] S. Manly,[1] W.A. Mann,[13] C. Mauger,[16] K.S. McFarland,[1] B. Messerly,[19] J. Miller,[14] J.G. Morfín,[7] D. Naples,[19] J.K. Nelson,[12] C. Nguyen,[20] A. Norrick,[12] Nuruzzaman,[17,14] A. Olivier,[1] V. Paolone,[19] G.N. Perdue,[7,1] M.A. Ramírez,[5] R.D. Ransome,[17] D. Ruterbories,[1] H. Schellman,[10,11] C.J. Solano Salinas,[21] H. Su,[19] M. Sultana,[1] V.S. Syrotenko,[13] E. Valencia,[12,5] D. Wark,[2] A. Weber,[2] M.Wospakrik,[20] B. Yaeggy,[14] and L. Zazueta[12]

(The MINERνA Collaboration)

[1] *University of Rochester, Rochester, New York 14627 USA*
[2] *Oxford University, Department of Physics, Oxford, United Kingdom*
[3] *Department of Physics, University of Minnesota – Duluth, Duluth, Minnesota 55812, USA*
[4] *AMU Campus, Aligarh, Uttar Pradesh 202001, India*
[5] *Campus León y Campus Guanajuato, Universidad de Guanajuato, Lascurain de Retana No. 5, Colonia Centro, Guanajuato 36000, Guanajuato México.*
[6] *Sección Física, Departamento de Ciencias, Pontificia Universidad Católica del Perú, Apartado 1761, Lima, Perú*
[7] *Fermi National Accelerator Laboratory, Batavia, Illinois 60510, USA*
[8] *University of Geneva, 1211 Geneva 4, Switzerland*
[9] *Centro Brasileiro de Pesquisas Físicas, Rua Dr. Xavier Sigaud 150, Urca, Rio de Janeiro, Rio de Janeiro, 22290-180, Brazil*
[10] *Department of Physics, Oregon State University, Corvallis, Oregon 97331, USA*
[11] *Northwestern University, Evanston, Illinois 60208*
[12] *Department of Physics, College of William & Mary, Williamsburg, Virginia 23187, USA*
[13] *Physics Department, Tufts University, Medford, Massachusetts 02155, USA*
[14] *Departamento de Física, Universidad Técnica Federico Santa María, Avenida España 1680 Casilla 110-V, Valparaíso, Chile*
[15] *IISER, Mohali, Knowledge city, Sector 81, Manauli PO 140306*
[16] *Department of Physics and Astronomy, University of Pennsylvania, Philadelphia, PA 19104*
[17] *Rutgers, The State University of New Jersey, Piscataway, New Jersey 08854, USA*
[18] *Massachusetts College of Liberal Arts, 375 Church Street, North Adams, MA 01247*
[19] *Department of Physics and Astronomy, University of Pittsburgh, Pittsburgh, Pennsylvania 15260, USA*
[20] *University of Florida, Department of Physics, Gainesville, FL 32611*
[21] *Universidad Nacional de Ingeniería, Apartado 31139, Lima, Perú*

(Dated: October 25, 2019)

Observables based on the final state kinematic imbalances are measured in the mesonless production of $\nu_\mu + A \to \mu^- + p + X$ in the MINERνA tracker. Components of the muon-proton momentum imbalances parallel (δp_{Ty}) and perpendicular(δp_{Tx}) to the momentum transfer in the transverse plane are found to be sensitive to the nuclear effects such as Fermi motion, binding energy and non-QE contributions. The QE peak location in δp_{Ty} is particularly sensitive to the binding energy. Differential cross sections are compared to predictions from different neutrino interaction models. None of the Fermi gas models simultaneously describe every feature of the QE peak width, location, and non-QE contribution to the signal process. Correcting the GENIE's binding energy implementation according to theory causes better agreement with data. Hints of proton left-right asymmetry is observed in δp_{Tx}. Better modelling of the binding energy can reduce bias in neutrino energy reconstruction and these observables can be applied in current and future experiments to better constrain nuclear effects.

PACS numbers: 13.15.+g,25.70.Bc,21.10.Dr

I. INTRODUCTION

Neutrino oscillation experiments measure the final state particles produced by neutrino-nucleus scattering processes. Models that accurately describe these interactions are crucial to reducing the uncertainties in the measurements of oscillation parameters.

Most neutrino-nucleus interactions are modeled through the impulse approximation (IA), where the probe sees the target nucleus as a collection of independent nucleons and the resulting particles then evolve independently. Important components of modeling in

the IA picture include the initial state nucleon's energy-momentum distributions, the nuclear potentials, and the final state interactions (FSIs) that modify the kinematics of the final-state particles as they propagate through the nucleus.

The leptonic system provides energy to the hadronic side of the reaction to bring a bound nucleon on-shell and separate it from the remnant nucleus. Such energy is often loosely referred to as "binding energy", but Reference [1] draws a distinction between the different energy parameters in neutrino models and how their effects depend on implementation details.

In this paper we refer to the average energy transferred to the target nucleus to bring a bound nucleon inside the target onto the mass shell as the "removal energy", represented in this paper by $\epsilon^{N(P)}$ for the neutron (proton) initial state in neutrino (antineutrino) interactions. The energy associated with nuclear potentials is referred to as the nuclear potential energy. The combined effects of the "removal energy" and the nuclear potential energy is referred to as the "interaction energy". The interaction energy implementation in the IA picture is discussed in detail in Sec. II.

It is very important to implement the interaction energy correctly or else it could produce a bias in the average neutrino energy reconstruction and in the modelling of the kinematics in the final state nucleons. The precise extraction of the mass-squared difference between 2 neutrino eigenstates (δm^2), for instance, by the long-baseline oscillation experiments can be achieved if there is no bias in the neutrino energy scale. Shifts in E_μ may have large effects for T2K, MicroBooNE, and for the second oscillation maximum in DUNE. Shifts in proton energy will affect most of the QE and Δ resonance region for all experiments that measure the proton in the final state.

This paper examines a set of new observable quantities with sensitivities to nuclear effects, especially to the interaction energy, and compares the measurements to existing neutrino Monte Carlo (MC) generators. The variables are extensions to the recent measurements of momentum imbalance in mesonless events with a muon and proton in the final state, here referred to as single transverse kinematic imbalance (single-TKI) [2] by the MINERνA [3] and T2K [4] experiments.

The new observables are derived from the single-TKI observable $\delta\mathbf{p}_{\mathrm{T}}$. Specifically, we define δp_{Ty} to be the projection of $\delta\mathbf{p}_{\mathrm{T}}$ along the transverse component of the leptonic momentum transfer, which is sensitive to the effects of the interaction energy. We also report on the cross section in δp_{Tx}, the $\delta\mathbf{p}_{\mathrm{T}}$ projection normal to the neutrino-muon interaction plane. The single-TKI variables and their sensitivities to the interaction energy is discussed in greater details in Sec. III and Sec. IV respectively.

These quantities provide neutrino oscillation experiments with a method to evaluate the validity of the interaction energy implemented in the interaction models. The interaction energy affects the reconstructed energy scale in the simulated neutrino interaction. Evaluating the uncertainties in the neutrino energy scale based on an inaccurate implementation of the interaction energy will result in unnecessarily large systematics.

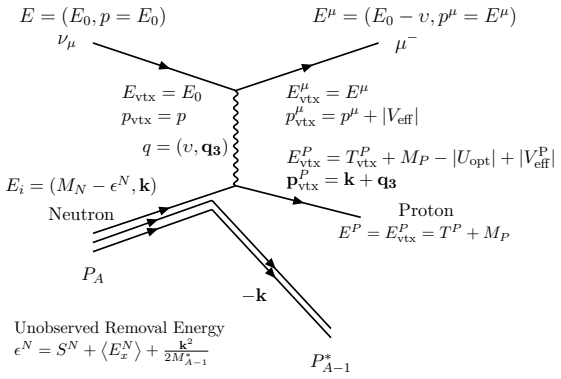

FIG. 1. A neutrino interaction with a bound neutron in the impulse approximation. ν, μ, N and P are the neutrino, muon, neutron and protons respectively. The incoming neutrino with 4-momentum E interacts with the bound neutron with 3-momentum $\mathbf{k}$ and removal energy ϵ^N. The removal energy consists of the nucleon separation energy S^N, average excitation energy $\langle E^N_x \rangle$ and the kinetic energy of the remnant nucleus. $E^{P(\mu)}$ and $p^{P(\mu)}$ are the proton (μ) total energy and momentum, T^P is the proton kinetic energy, $|U_{\mathrm{opt}}|$ and $|V^{\mathrm{P}}_{\mathrm{eff}}|$ ($|V_{\mathrm{eff}}|$) are the magnitudes of the optical potential and the Coulomb potential experienced by proton (muon). The quantities with the subscript (vtx) are those immediately after 4-momentum transfer.

We measure δp_{Tx} and δp_{Ty} using MINERνA ν_μ-induced muon-proton mesonless interactions on hydrocarbon at $\langle E_\nu \rangle = 3$ GeV; this is the same data set as was studied previously in Ref [3]. The differential cross sections in these quantities are compared with GENIE [5], NEUT 5.40 [6], NuWro [7] and GiBUU [8, 9] event generator predictions. The methodology is detailed in Sec. V and the results are discussed in Sec. VI.

II. IMPULSE APPROXIMATION

We illustrate the effects of interaction energy with the charged-current quasielastic (CCQE) interaction in the IA picture shown in Fig. 1. In this picture, only a single nucleon is involved in the hard scattering, $\nu\mathrm{n} \to \mu^-\mathrm{p}$.

The neutrino with energy E_0 made 4-momentum transfer, $q = (\upsilon, \mathbf{q_3})$ to a bound neutron of mass M_N inside a target nucleus with A nucleons, where υ (also called ω or q_0 in the literature) and $\mathbf{q_3}$ are the energy and momentum transfer respectively. The target nucleus was initially at rest with mass M_{A}, the bound neutron has 4-momentum $E_i = (M_N - \epsilon^N, \mathbf{k})$ where $\mathbf{k}$ is neutron's Fermi momentum. The remnant nucleus with 4-momentum P^*_{A-1} must have momentum $-\mathbf{k}$ for the target nucleus to be at rest. The energy of the initial state neutron can

be written as:

$$E_i = M_{\rm A} - \sqrt{{M^*_{\rm A-1}}^2 + \mathbf{k}^2}, \quad (1)$$

where $M^*_{\rm A-1}$ is the mass of the excited spectator nucleus. For the nuclear targets typically used in neutrino experiments (^{12}C, ^{16}O and ^{40}Ar), we have ${M^*_{\rm A-1}}^2 \gg \mathbf{k}^2$. Then we can expand the initial state nucleon energy as:

$$\begin{aligned} E_i &\approx M_{\rm A} - M^*_{\rm A-1} - \frac{\mathbf{k}^2}{2M^*_{\rm A-1}} \\ &= M_N - S^N - E_x^N - \frac{\mathbf{k}^2}{2M^*_{\rm A-1}}. \end{aligned} \quad (2)$$

The removal energy parameter

$$\epsilon^N = S^N + E_x + \langle T_{A-1} \rangle \,, \quad (3)$$

accounts for the *neutron separation energy* from the target nucleus S^N,

$$S^N = M_{A-1} + M_N - M_A, \quad (4)$$

and the excitation energy of the final state nucleus, E_x,

$$E_x = M^*_{A-1} - M_{A-1}. \quad (5)$$

The average kinetic energy $\langle T_{A-1} \rangle = \mathbf{k}^2/(2M^*_{\rm A-1})$ of the excited remnant nucleus with A-1 nucleons affects the interaction only through its nuclear potentials. For typical ν QE interactions on ^{12}C, $S^N = 18.7$ MeV, $E_x^N = 10.1$ MeV and $\langle T_{A-1} \rangle = 1.4$ MeV [1]. The removal energy is the average energy needed to bring the neutron onto the mass-shell.

There are additional effects associated with the nuclear potentials that should be accounted for. For example, the nuclear optical potential describes the nucleus as a medium with complex refractive index: the real part of the potential affects the allowed kinematics of the initial state lepton-nucleon system in the IA while the imaginary part is related to inelastic scattering as the outgoing nucleon is making an exit from the nucleus [10]. Reference [1] fits inclusive electron scattering data to determine the real part of the optical potential which depends on the 3-momentum of the outgoing nucleon at the interaction vertex and is denoted as $U_{\rm opt}[(\mathbf{k}+\mathbf{q}_3)^2]$ in this work. The effect of the optical potential is largest at lower momentum. For carbon, the parameterization of Reference [1] is

$$U_{\rm opt} = \min\left[0, -29.1 + (40.9/{\rm GeV}^2)(\mathbf{k}+\mathbf{q}_3)^2)\right] \ {\rm MeV}. \quad (6)$$

In this analysis we use this parameterization, and it is on average 2 MeV for our selected events.

Another potential, the Coulomb potential $V_{\rm eff}$ of the positively charged remnant nucleus will modify the momenta of the outgoing charged particles as they propagate through the nucleus. In Fig. 1, a distinction between the Coulomb potential experienced by muon ($|V_{\rm eff}|$) and proton ($|V^{\rm P}_{\rm eff}|$) is made; however,for neutrino interactions both particles experience the same Coulomb potential as the proton number in the nucleus remains unchanged after the interaction. For carbon, $|V_{\rm eff}|$ is 3.1 MeV [1].

Figure 1 illustrates energy and momentum conservation between the initial and final state. The total energy of the final proton and muon is equal to the total of the initial neutron and lepton, less energy required to create the final state excited nucleon in the reaction. The Coulomb potential affects any charged final state particles, but the optical potential affects the final state nucleon only. For example, the muon with total energy $E^\mu = E^\mu_{\rm vtx}$ begins inside the Coulomb potential, with kinetic energy $E^\mu + |V_{\rm eff}|$ and potential energy $-|V_{\rm eff}|$, and is decelerated during transport inside the nucleus medium so that its kinetic energy is E^μ outside the nucleus. The proton experiences both the Coulomb potential and the optical potential, which modify its kinetic energy and momentum but conserve the total energy. The full energy conservation equation on the hadronic side is as follows [1]:

$$\begin{aligned} E^P_{\rm vtx} = \upsilon + M_N - S^N - E_x^N - \frac{\langle \mathbf{k}^2 \rangle}{2{M^*_{A-1}}^2} = \\ \sqrt{(\mathbf{k}+\mathbf{q_3})^2 + M_P^2} - |U_{\rm opt}[(\mathbf{k}+\mathbf{q_3})^2]| + |V^{\rm P}_{\rm eff}| \\ = E^P. \end{aligned} \quad (7)$$

Here, the final state proton is assumed to be on-shell with energy $E^P_{\rm vtx} = E^P_f$,before and after exiting the nuclues. Its kinetic energy immediately after the 4-momentum transfer is

$$T^P_{\rm vtx} = \upsilon + M_N - M_P - \epsilon^N, \quad (8)$$

and is modified by the nuclear potentials so that outside the nucleus the kinetic energy becomes

$$T^P = T^P_{\rm vtx} - |U_{\rm opt}| + |V^{\rm P}_{\rm eff}|. \quad (9)$$

The removal energy used by neutrino Monte Carlo (MC) generators, such as GENIE [5], NEUT [6], and NuWro [7], are discussed in detail in Reference [1]. These generators use variants of spectral functions, mostly the Fermi gas model in the IA picture with removal energy constrained by inclusive electron scattering data [11]. However, they have distinct implementations of the IA model which affects the energy terms going into the removal energy parameter. For example, in GENIE's IA implementation, the off-shell bound initial nucleon is generated with Eq.(7), but with E_x^N, $U_{\rm opt}$, and $V^{\rm P}_{\rm eff}$ set to 0. GENIE subtracts an additional "binding energy" parameter $\Delta^{\rm nucleus}_{\rm GENIE}$ from the final state protons in QE processes to account for the removal energy. The implementation of this term is independent of the kinematics at the interaction vertex, which causes the energy of the final state nucleons to be biased. The values of $\Delta^{\rm nucleus}_{\rm GENIE}$

were measured by Reference [11] and referred to as the "Moniz interaction energy" in Reference [1]. The Moniz interaction energy is an empirical fit to the sum of the removal energy and the nuclear potentials, but for a non-relativistic on-shell formalism. For ν+^{12}C scattering, $\Delta^{\mathrm{C}}_{\mathrm{GENIE}} = 25$ MeV [5].

In this paper, we refer to the collective energy shifts due to removal energy and the nuclear potentials as the "interaction energy", in the spirit of the Moniz interaction energy of Reference [1]. This interaction energy is specific to the off-shell formalism described in Eq. 7.

We simulate the effects of the interaction energy implementations in GENIE by modifying the final state muon and proton energies after a sample is generated according to Table I. The corrections outlined are motivated by the study in Reference [1]. Comparisons between the default GENIE implementation (Mode 00) and two different corrections (Mode 01 and 02) are made. For both sets of corrections, which are applied to QE events, we add $\Delta^{\mathrm{C}}_{\mathrm{GENIE}}$ back to the exiting proton to undo the bias, we then subtract E_x from the muon to account for the shift in momentum transfer in the leptons (derived in Appendix A). In addition, Mode 01 applies an optical potential correction to both the muon and proton, while Mode 02 applies the Coulomb correction on top of Mode 01. The average $|U_{\mathrm{opt}}|$ is ≈ 2 MeV for the proton and muon kinematics chosen. Table I shows the shifts in the average peak positions in the quantity δp_{Ty}, defined in Eq. 12 caused by these corrections.

These corrections are approximations to the leading order effects in model level implementations. Model level implementations will also cause subtle changes to the direction distributions of the final state particles, but their effects are small. Appendix A outlines the derivation of these corrections.

III. THE SINGLE-TKI VARIALBES

The single-TKI measurements for CCQE-like events, which include a lepton, at least one proton and no mesons in the final state, are defined in Reference [2]:

$$\delta\mathbf{p}_{\mathrm{T}} \equiv \mathbf{p}^{\mathrm{p}}_{\mathrm{T}} + \mathbf{p}^{\mu}_{\mathrm{T}}, \tag{10}$$

$$\delta\alpha_{\mathrm{T}} \equiv \arccos\left(-\hat{\mathbf{p}}^{\mu}_{\mathrm{T}} \cdot \hat{\delta\mathbf{p}_{\mathrm{T}}}\right), \tag{11}$$

where $\mathbf{p}^{\mathrm{p}}_{\mathrm{T}}$ and $\mathbf{p}^{\mu}_{\mathrm{T}}$ are the components of proton and muon momenta in the plane perpendicular to the neutrino direction. The single-TKI variable $\delta\mathbf{p}_{\mathrm{T}}$ and its decompositions along the Cartesian coordinate system defined with respect to the neutrino and muon kinematics are illustrated in Fig. 2 and mathematically defined as

$$\begin{aligned}\delta p_{\mathrm{Tx}} &= (\hat{\mathbf{p}}_{\nu} \times \hat{\mathbf{p}}^{\mu}_{\mathrm{T}}) \cdot \delta\mathbf{p}_{\mathrm{T}},\\ \delta p_{\mathrm{Ty}} &= -\hat{\mathbf{p}}^{\mu}_{\mathrm{T}} \cdot \delta\mathbf{p}_{\mathrm{T}}.\end{aligned} \tag{12}$$

Here, $\hat{\mathbf{p}}_{\nu}$ is the neutrino direction, δp_{Ty} is anti-parallel to the muon transverse direction $\hat{\mathbf{p}}^{\mu}_{\mathrm{T}}$ while δp_{Tx} is perpendicular to δp_{Ty} along the normal of neutrino-muon plane. The coordinate system describing δp_{Tx} and δp_{Ty} is relative to the neutrino and muon kinematics. Specifically $\hat{\mathbf{y}}$ is along the transverse component of 3-momentum transfer, $\hat{\mathbf{z}}$ is along the neutrino direction and there is no 3-momentum transfer in the $\hat{\mathbf{x}}$ direction. Both δp_{Tx} and δp_{Ty} can be measured from the final state particles. Any interaction energy effect will mostly affect the 4-momentum transfer and δp_{Ty}. For CCQE events, δp_{Tx} is expected to symmetrically distribute on both sides of the neutrino-muon interaction plane.

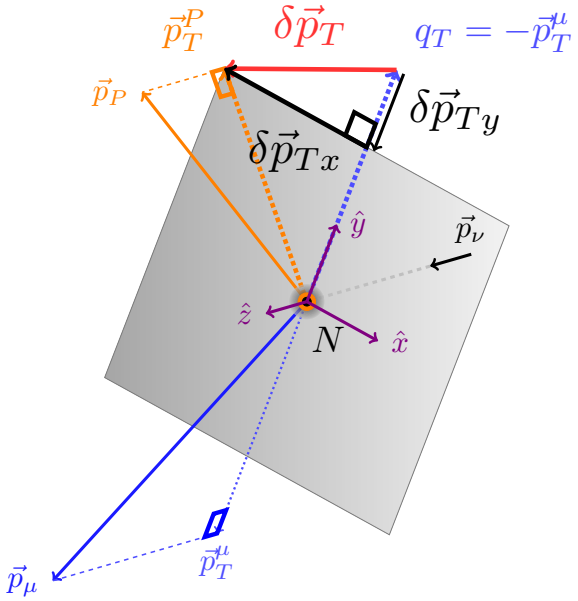

FIG. 2. Schematics of the Single Transverse Kinematic Imbalances and their projections.The incoming neutrino interacts on the neutron (N) in the nucleus. The neutrino direction $\hat{\mathbf{p}}_{\nu}$ forms the z axis. A final state muon with $\mathbf{p}_{\mu}$ and a proton with $\mathbf{p}_{p}$ are produced. The muon transverse momentum is $\mathbf{p}^{\mu}_{\mathrm{T}}$, and $-\hat{\mathbf{p}}^{\mu}_{\mathrm{T}}$ defines the y axis. The proton transverse momentum is $\mathbf{p}^{\mathrm{p}}_{\mathrm{T}}$ and decomposed along x and y axis respectively. In this example, both δp_{Tx} and δp_{Ty} are negative, and only the distribution of δp_{Tx} for QE events is expected to be symmetric around zero.

$(\delta p_{\mathrm{Tx}}, \delta p_{\mathrm{Ty}})$ can be defined in terms of $(\delta p_{\mathrm{T}}, \delta\alpha_{\mathrm{T}})$ as:

$$\begin{aligned}|\delta p_{\mathrm{Tx}}| &= \delta p_{\mathrm{T}} \sin\delta\alpha_{\mathrm{T}},\\ \delta p_{\mathrm{Ty}} &= \delta p_{\mathrm{T}} \cos\delta\alpha_{\mathrm{T}}.\end{aligned} \tag{13}$$

Here δp_{Ty} is positive if the proton has gained momentum along $-\mathbf{p}^{\mu}_{\mathrm{T}}$. Figure 3 illustrates the relationship between $(\delta p_{\mathrm{Tx}}, \delta p_{\mathrm{Ty}})$ and $(\delta p_{\mathrm{T}}, \delta\alpha_{\mathrm{T}})$ as the different projections of $\delta\mathbf{p}_{\mathrm{T}}$ in the Cartesian and the polar coordinate systems respectively. A shift in the interaction energy changes the position of the quasielastic(QE) peak along the $\hat{\mathbf{y}}$ direction. The resulting distribution in the $\delta\alpha_{\mathrm{T}}$ and δp_{T} residuals provides insights into other nuclear effects affecting the cross section, such as FSIs, the Fermi motion

TABLE I. Calculated energy corrections to the final state leptons and hadrons from the GENIE generator for QE neutrino scattering on ^{12}C, $\Delta^{\rm C}_{\rm GENIE} = 25$ MeV, $E_x = 10.1$ MeV. Other interaction channels are not altered.

Correction	$E^P = E^P_{\rm GENIE} + \delta^P$ δ^P (MeV)	$E^\mu = E^\mu_{\rm GENIE} + \delta^\mu$ δ^μ (MeV)	GENIE Baseline Shift $\langle\delta^P\rangle$,$\langle\delta^\mu\rangle$ (MeV)	QE Baseline Shift $\langle\delta p_{\rm Ty}\rangle$(MeV/$c$)
00: Default (no corrections)	0	0	0,0	0
01: $U_{\rm opt}$ only (w/ E_x&$\Delta^{\rm C}_{\rm GENIE}$)	$\Delta^{\rm C}_{\rm GENIE} - \lvert U_{\rm opt}\rvert$	$\lvert U_{\rm opt}\rvert - E_x$	22.7, −7.8	16.1
02: $U_{\rm opt}$ and $V_{\rm eff}$ (w/ E_x&$\Delta^{\rm C}_{\rm GENIE}$)	$\Delta^{\rm C}_{\rm GENIE} - \lvert U_{\rm opt}\rvert$ $+\lvert V^{\rm P}_{\rm eff}\rvert$	$\lvert U_{\rm opt}\rvert - E_x$ $-\lvert V_{\rm eff}\rvert$	25.8, −10.9	18.5

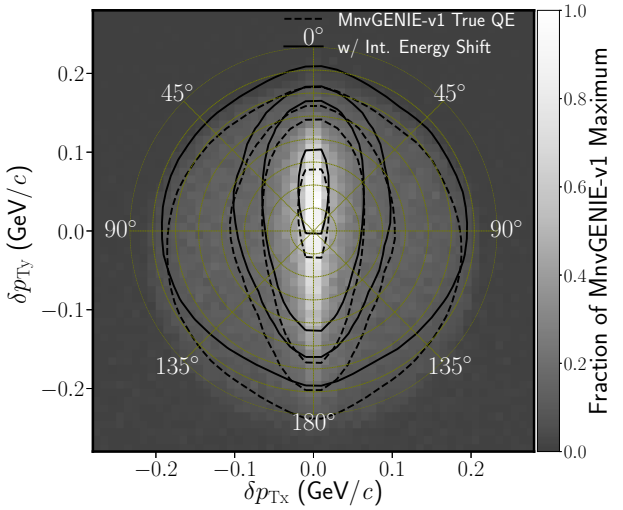

FIG. 3. $\delta p_{\rm Ty}$ vs. $\delta p_{\rm Tx}$ for CCQE events in GENIE. The contours, from outside towards the center, represent 0.1, 0.2, 0.3, and 0.7 of maximum. The angles correspond to $\delta\alpha_{\rm T}$ values. The neutrino direction points out of the page. The dashed contour describes the default GENIE distribution with a MnvGENIE-v1 tune. The solid contour shows the shift in the distribution after correction is made to the interaction energy with correction 01 of Table I. There is negligible deformation in the $\delta p_{\rm Tx}$ direction compared to the shift in $\delta p_{\rm Ty}$.

and 2p2h processes[3].

IV. SENSITIVITIES TO INTERACTION ENERGY

The shape of $\delta p_{\rm Tx}$ and $\delta p_{\rm Ty}$ are results of nuclear effects. The non-zero width of $\delta p_{\rm Tx}$ for the QE portion of the signal should be be largely due to the Fermi motion of the target nucleus. QE events affected by direction changing FSIs and background events from non-QE processes produce a population of events predicted to have an even broader distribution in $\delta p_{\rm Tx}$ than Fermi motion produces. As all of the momentum transferred to the hadronic system is confined in the yz plane, changes to the interaction energy at the event vertex must manifest through $\delta p_{\rm Ty}$. Our corrections do not capture the full kinematic effects that would also modify the angular distributions.

We present an illustration of the the variables' sensitivities to the interaction energy. For an outgoing nucleon with energy E'_f before it has left the region of nuclear potentials, its momentum $\mathbf{p}_f$ as a function of an energy shift τ due to the interaction energy is:

$$|\mathbf{p}_f(\tau)| = \sqrt{(E'_f - \tau)^2 - M_P^2}, \tag{14}$$

where $E'_f = \sqrt{M_P^2 + \mathbf{p}_0^2}$ and $\mathbf{p}_0 = \mathbf{p}_f(0) = \mathbf{k} + \mathbf{q}$. In the limit

$$\frac{\tau E'_f}{p_0^2} \ll 1, \tag{15}$$

we can approximate $\mathbf{p}_f(\tau)$ by

$$\mathbf{p}_f(\tau) \approx \left(1 - \frac{E'_f}{p_0^2}\tau\right)\mathbf{p}_0. \tag{16}$$

Defining $\alpha = \tau E'_f/p_0^2$, we can write the 4-momentum conservation equation without FSI as:

$$\begin{pmatrix} \upsilon \\ 0 \\ q_T \\ q_L \end{pmatrix} + \begin{pmatrix} E_i \\ k_x \\ k_y \\ k_z \end{pmatrix} \approx \begin{pmatrix} E'_f \\ p_{0x} \\ p_{0y} \\ p_{0z} \end{pmatrix} - \begin{pmatrix} \tau \\ \alpha p_{0x} \\ \alpha p_{0y} \\ \alpha p_{0z} \end{pmatrix}, \tag{17}$$

where $(0, q_T, q_L)$ are components of the 3-momentum transfer $\mathbf{q}$, (k_x, k_y, k_z) are components of Fermi motion $\mathbf{k}$. In this picture, q_T is directly measurable as the transverse component of muon momentum, with magnitude $p^\mu_{\rm T}$, but q_L cannot be directly measured and estimates depend on the model used to calculate neutrino energy.

The transverse components of the 3-momentum imbalance are

$$\begin{aligned} \delta p_{\rm Tx} &= (1-\alpha)p_{0x} \\ &\approx k_x - \alpha p_{0x} = k_x - \tau\frac{E_f}{p_0^2}p_{0x}, \end{aligned} \tag{18}$$

$$\begin{aligned} \delta p_{\rm Ty} &= (1-\alpha)p_{0y} + \mathbf{p}_\mu \cdot \hat{\mathbf{y}} \\ &= p_{0y} - p^\mu_T - \alpha p_{0y} = p_{0y} - q_T - \alpha p_{0y} \\ &\approx k_y - \alpha p_{0y} = k_y - \tau\frac{E_f}{p_0^2}p_{0y}. \end{aligned} \tag{19}$$

In the limit $\tau, \alpha \to 0$, δp_{Tx} and δp_{Ty} are the transverse components of the Fermi momentum, (k_x, k_y). The effect of energy shift, τ, in each component of $(\delta p_{\mathrm{Tx}}, \delta p_{\mathrm{Ty}})$ is then proportional to that component of p_0. When $p_T^{\mu} \gg k_y$, the shift in δp_{Ty} will be larger than the shift in δp_{Tx}. In both components, the interaction energy effects acting on the Fermi momentum will average to zero, whereas the effects on δp_{Ty} from q_T will yield a net average shift in δp_{Ty}. For events in GENIE2.12.10, there is approximately $+15$ MeV/c offset in δp_{Ty}.

V. APPARATUS AND METHODOLOGY

The measurements of differential cross sections in δp_{Tx} and δp_{Ty} with the MINERνA detector [12] use the same sample and methodology of the measurements described in Reference [3]. The signal requires no pions, one muon, and at least one proton in the final state, satisfying

$$\begin{cases} 1.5 \text{ GeV}/c < p_{\mu} < 10 \text{ GeV}/c, \ \theta_{\mu} < 20^{\circ}, & (20) \\ 0.45 \text{ GeV}/c < p_{\mathrm{p}} < 1.2 \text{ GeV}/c, \ \theta_{\mathrm{p}} < 70^{\circ}, & (21) \end{cases}$$

where p_{μ} and θ_{μ} (p_{p} and θ_{p}) are the final-state muon (proton) momentum and opening angle with respect to the neutrino direction, respectively. The data set corresponds to $3.28{\times}10^{20}$ protons on target (POT) delivered between 2010 and 2012 by the NuMI beam line [13] at Fermilab. For this beam, the integrated ν_{μ} flux is predicted to be $2.88 \times 10^{-8}/\mathrm{cm}^2/\mathrm{POT}$[14].

Reconstructed events with one muon and at least one proton in the MINERνA tracker satisfying Eq.(20)-(21) are selected. A sub-sample is selected to favor elastically scattered and contained (ESC) protons in the CH tracker of the detector [3, 15] to improve p_{p} resolution. After the event selection, background contributions are subtracted using predictions from GENIE 2.8.4, which is fitted with a data-driven method [16]. The resulting distributions are then unfolded to account for detector resolution effects in the measurement of δp_{Tx} and δp_{Ty} [3, 17]. This technique uses four iterations to balance model bias and statistical uncertainties in the unfolded distribution. The event distributions are then corrected for detector efficiency predicted by the simulation and normalized by the the number of target nucleons (3.11×10^{30}) and the predicted ν_{μ} flux to obtain the flux-averaged differential cross sections.

Neutrino interactions are simulated with GENIE 2.8.4 [5] in both a nominal form, and also with a MINERνA "tune" (MnvGENIE-v1.0.1). The nominal GENIE generates initial states with a modified Fermi Gas model containing contributions from the Bodek-Ritchie tail [18]. The CCQE kinematics are modelled by Llewellyn Smith [19] and a dipole form factor using $M_A^{QE} = 0.99$ GeV/c^2. The resonant pion productions are modelled by Rein and Sehgal [20]. The non-resonant pion production originally included by Rein-Sehgal model is modelled by Deeply Inelastic Scattering (DIS) process through a Quark-Parton Model parameterized with the Bodek-Yang structure functions [21]. FSIs are simulated with the GENIE hA model.

TABLE II. Uncertainties in 50 MeV/c-wide bins of δp_{Tx} and δp_{Ty}. The uncertainties for "peak" bins are taken from the bins nearest 0 MeV/c, and the "edge" bins are those from $\pm$150 to $\pm$200 MeV/c. For $|\delta p_{\mathrm{T}}| > 200$ MeV/c, non-CCQE contributions begin to dominate. The uncertainties for δp_{Ty} at the edge is taken from the positive δp_{Ty} side, rather than the negative δp_{Ty} side where the uncertainties are smaller.

Percentage uncertainties	Position	δp_{Tx}	δp_{Ty}
Stat(%)	peak	5	4
	edge	9	8
Flux(%)	peak	6	6
	edge	5	6
Background Model(%)	peak	7	7
	edge	10	12
Detector(%)	peak	6	6
	edge	5	17
Total(%)	peak	12	12
	edge	15	22

The tuning is based on MnvGENIE-v1, which has been applied in previous publications. MnvGENIE-v1 includes the Valencia two-particle-two-holes (2p2h) model [22–24] for two-body current simulation. Furthermore, the interaction strength of this 2p2h model has been tuned to MINERνA inclusive scattering data [25], resulting in a significant enhancement relative to the Valencia model in a restricted region of energy-momentum transfer. MnvGENIE-v1 also includes a non-resonant pion reduction to 43% of the nominal as constrained by comparisons with bubble chamber deuterium data [26, 27]. There is also a modification to the collective excitations of the nucleus for the CCQE channel, approximated as a superposition of 1p1h excitations and calculated with the Random Phase Approximation (RPA) in Reference [28] and uncertainties in Reference [29]. The effects of non-resonant pion production and RPA in this analysis are negligible.

Uncertainties on $\delta p_{\mathrm{Tx}}(\delta p_{\mathrm{Ty}})$ result from statistical fluctuations and uncertainties in the NuMI flux prediction, the GENIE background model, and the detector response. The uncertainties from the peak bins and edge bins from $\delta p_{\mathrm{Tx}}(\delta p_{\mathrm{Ty}})$ are summarized in Table II. The unfolding technique minimizes the effect of the signal model on the unfolded cross section, as long as the signal model is approximately correct. This class of uncertainties is negligible here. See Appendix B for an example which required more care.

VI. RESULTS AND DISCUSSIONS

Model comparison is facilitated with the NUISANCE [30] neutrino interaction cross section comparison package. For the primary comparison with data, we use GENIE 2.12.10 with the Valencia 2p2h model replacing the

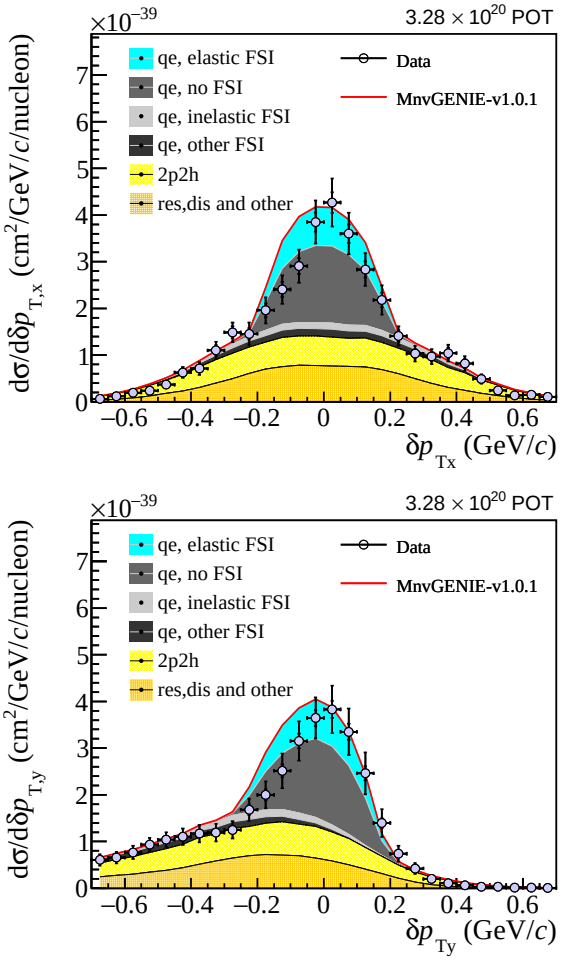

FIG. 4. Differential cross sections in δp_{Tx} (top) and δp_{Ty} (bottom) compared to MnvGENIE-v1.0.1The MnvGENIE-v1.0.1 histogram is separated into the GENIE defined QE, 2p2h and non-QE event types. The QE region is further separated into the GENIE FSI experienced by the selected proton before exiting the nucleus. The QE elastic FSI regions displayed in the figures are replaced by the no FSI contributions scaled to 50%. Note δp_{Tx} seems to be slightly asymmetric about the center. The δp_{Ty} peak is shifted to the left and has larger width than data.

default empirical 2p2h model. NUISANCE is used to apply the MnvGENIE-v1.0.1 tune that is described above. GENIE 2.12.10 and GENIE 2.8.4 have consistent model implementations. A careful internal MINERνA study indicates the main difference for this analysis is an increase of S^N by 14.8 MeV from changes to the nuclear masses in GENIE.

The unfolded cross section results are shown in Fig 4. The δp_{Tx} and δp_{Ty} cross sections are in the top and bottom panels respectively. There are significant non-QE contributions for both distributions. Of these about half are due to the tuned 2p2h. For each cross section, the QE distribution is broken down into the generated FSI modes. Here, the GENIE no FSI means the final state nucleon exited the nucleus without interaction, and the inelastic FSI implies the inelastic knockout of a second nucleon. The other FSI category includes channels such as charge exchange multi-nucleon knockout, and pion production/absorption during nucleon transport. Finally, the elastic FSI originally means nucleon-nucleus elastic scattering. The prediction for nucleon version of the elastic FSI intended to involve scattering angles less than 10°. To approximate the intended implementation, the original elastic FSI events were eliminated and the events with no FSI were weighted up to 1.50 to compensate. The elastic FSI contribution in the figure is equal to 50% of the no FSI contribution.

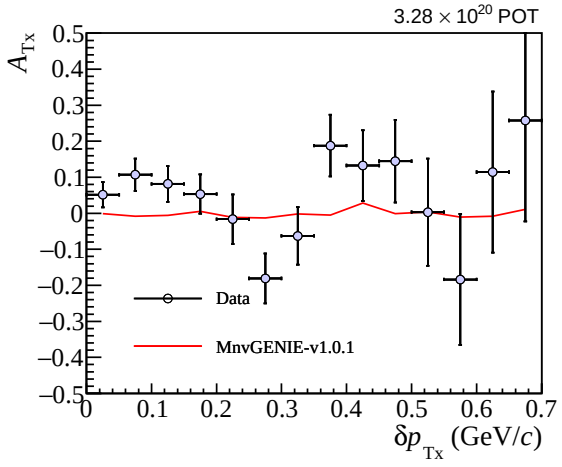

FIG. 5. The bin-by-bin asymmetry in the differential cross sections between $\pm|\delta p_{\mathrm{Tx}}|$ bins (Eq. 22). Data is compared to MnvGENIE-v1.0.1, which is representative of the other MC generators used in this study and exhibits no asymmetry.

A. Distribution in δp_{Tx}

The δp_{Tx} prediction is wider than the data in the peak region. While the reweighted elastic FSI does not faithfully reproduce a "fixed" elastic FSI, the width of the predicted no FSI contribution alone is higher than the data. If we assume no significant deviation in the non-QE distributions, then the discrepancy could imply an overestimation of the Carbon Fermi momentum and/or a reduction in the total fraction of the no FSI contribution.

Besides the width discrepancy, the data distribution in δp_{Tx} visually leans towards the positive side.

To measure the significance of the asymmetry, we define the bin-by-bin asymmetry between the positive and negative sides of the differential cross section in δp_{Tx} as:

$$A_{\mathrm{Tx}}(|\delta p_{\mathrm{Tx}}|) = \frac{\sigma_+ - \sigma_-}{\sigma_+ + \sigma_-}, \tag{22}$$

where $\sigma_\pm$ is the cross section at either $\pm|\delta p_{\mathrm{Tx}}|$ bin. The resulting distribution is reported in Fig 5, where

TABLE III. χ^2 of asymmetries (A_{Tx}) against no asymmetry case for regions of δp_{Tx} distributions calculated with the covariance matrix.

δp_{Tx} Range (GeV)	χ^2/ndf
$0.00 \sim 0.40$	19.9/8
$0.40 \sim 0.70$	4.95/7
$0.00 \sim 0.70$	21.6/15

observation of bin-by-bin asymmetries in the data and their significances in different ranges of δp_{Tx} are reported in Table III. None of the generators used in this study reproduce the asymmetric feature, where MnvGENIE-v1.0.1 is shown as an example.

The total asymmetry is defined as:

$$A_{\mathrm{LR}} = \frac{N_- - N_+}{N_- + N_+}, \tag{23}$$

with $N_{-/+}$ being the integrated cross sections on the left/right side of the neutrino-muon plane. The result is

$$A_{\mathrm{LR}} = -0.05 \pm 0.02,$$

where the uncertainty is propagated through the covariance matrix in the Supplemental Material.

Such an asymmetry could be caused by the pion absorption contributions to the signal [31]. Measurements of single-pion production at low energy in deuterium [32] and single-π^0 production by MINERνA [33] have seen positive pion asymmetries about the neutrino-muon plane. The correlated proton angular distributions in this measurement, from the resonant production with an unobserved absorbed pion, could exhibit an opposite asymmetry.

B. Distribution in δp_{Ty}

A similar width discrepancy to that of δp_{Tx} exists for δp_{Ty}, but there is an additional peak shift probably due to the interaction energy implementation in GENIE.

We demonstrate how modifying the interaction energy implementation affect the δp_{Tx} and δp_{Ty} variables. The two sets of corrections proposed in Table I are made to the final states muons and protons in MnvGENIE-v1.0.1' CCQE contribution in the MC sample.

Corrections 01, with U_{opt} correction only, and 02, with both U_{opt} and $|V_{\mathrm{eff}}|$ corrections, are shown in Fig. 6. The effects of U_{opt} is on the order of 2 MeV as it mainly affects nucleons at low kinetic energies.

The average δp_{Ty} shifts in the predicted QE contributions are 16.1 MeV/c and 18.5 MeV/c respectively. Significant fraction of the shift comes from adding the Moniz interaction energy for Carbon ($\Delta^{\mathrm{C}}_{\mathrm{GENIE}}$) back to the final state proton, and the removal of the average excitation energy ($\langle E_x \rangle$) from the muon.

The ratios, in the lower panels of Fig 6, of the corrected models and the data to MnvGENIE-v1.0.1 show the same upward-going trend in the QE peak region between $|\delta p_{\mathrm{Ty}}| < 0.2$ GeV. This trend is characteristic of a peak shift, and the similarities lend confidence to the validity of the theoretically motivated corrections.

Figure 7 and Fig. 8 compares NuWro Local Fermi Gas (LFG), NuWro Spectral Function (SF), GiBUU, the nominal GENIE, MnvGENIE-v1.0.1, as well as NEUT SF and LFG, distributions normalized to data cross sections. In terms of δp_{Ty}, the nominal GENIE with Nieves 2p2h does not depart much from the overall peak offset seen in MnvGENIE-v1.0.1, the ratio between which is nearly flat. Therefore the modifications to the 2p2h fraction, the non-resonant pion reweighting and RPA introduced by the MINERνA tune has little effect on the position of the peak. Data to MnvGENIE-v1.0.1 ratio, and in fact the ratios of all other models to MnvGENIE-v1.0.1, except NuWro LFG follow very similar trends. The NuWro SF and GiBUU models both have better agreements with data while NuWro LFG has overall disagreement in cross section.

The NuWro models include nuclear effects such as Pauli blocking, the Coulomb potential and an effective potential simulating the optical potential. The effective potential is validated against electron scattering data on targets including ^{16}O [34], a nucleus similar to ^{12}C [1]. The NuWro LFG has larger disagreement with the data. However, the average Fermi motion of typical LFG models the width lower than the Fermi-level of a regular Fermi gas. This produces a narrowness more suggestive of the data even if the complete model is not better.

The NEUT SF describes the QE peak location well, while the LFG shifts the peak location by more than 1σ. In fact NEUT SF describes both δp_{Tx} and δp_{Ty} very well near the peak regions.Unlike the NuWro variant, NEUT LFG predicts wider QE width in δp_{Ty} while at the same time produces width in δp_{Tx} comparable to that of the data.

GiBUU models the initial state nucleons with a local Thomas-Fermi approximation, and the nucleons are bound in a mean-field potential, where Pauli blocking is naturally simulated. The final state particles propagate through the nuclear medium are subject to a scalar potential that usually depend on both the nucleon momentum and nuclear density [35]. These features of GiBUU do not contribute to an especially superior description of the QE peak. Unrelated to the description of the peak, the tail distributions of the single-TKI quantities are sensitive especially to the 2p2h component and pion production followed by pion absorption with proton knockout. With a lower proton threshold than this analysis, it could include significant amounts of QE events followed by FSI. GiBUU seems to be quite adept at predicting three of the four tails of these signal distributions, while the other generators systematically overestimate these regions.

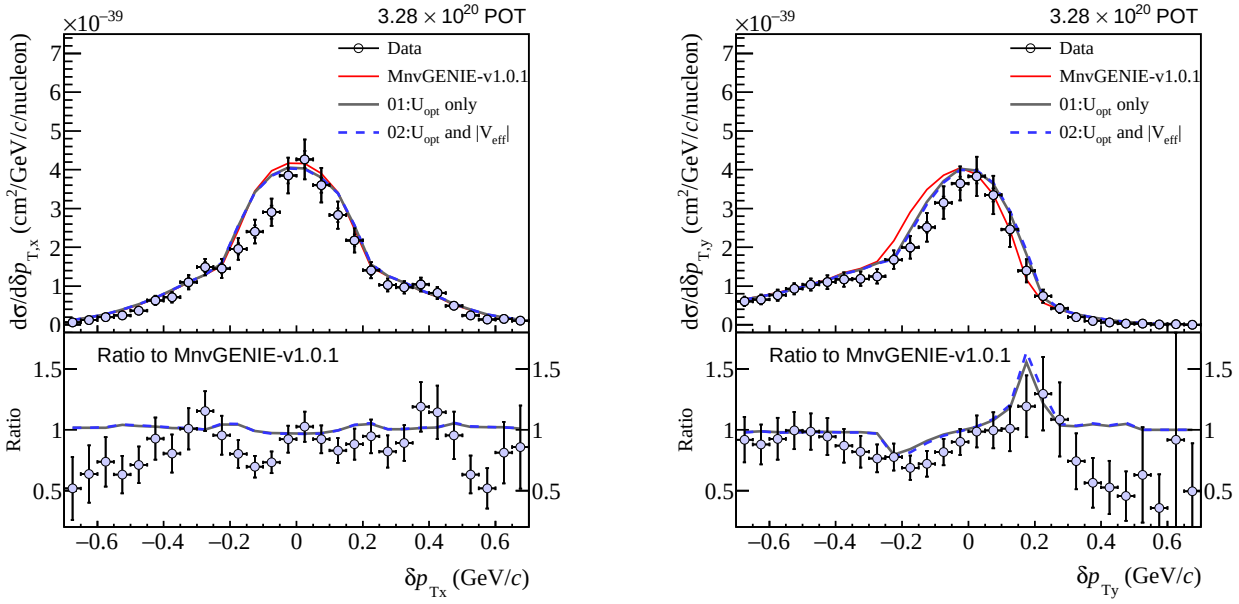

FIG. 6. Differential cross sections in $(\delta p_{\mathrm{Tx}}, \delta p_{\mathrm{Ty}})$ compared with MnvGENIE-v1.0.1 interaction energy corrections, defined in Table I. The corrections minimally affect δp_{Tx}, while bringing the δp_{Ty} peak region into closer agreement with data. Note the similar trends in δp_{Ty} ratios between the corrections and data.

Quantitative measure of agreements between the predicted and measured δp_{Ty} is done with a weighted averages, $\langle \delta p_{\mathrm{Ty}} \rangle$, defined as

$$\langle \delta p_{\mathrm{Ty}} \rangle = \frac{\sum_i \sigma_i \delta p_{\mathrm{Ty}_i}}{\sum_j \sigma_j}, \tag{24}$$

$$V = \frac{\sum_{i,j} \delta p_{\mathrm{Ty}_i} C_{ij} \delta p_{\mathrm{Ty}_j}}{(\sum_k \sigma_k)^2}, \tag{25}$$

$$\tag{26}$$

where σ_i and δp_{Ty_i} are the cross section and position in the i-th δp_{Ty} bin, i, j span over the summed range. The calculation of the variance V takes into account the correlated covariance matrix C_{ij}.

The computation of $\langle \delta p_{\mathrm{Ty}} \rangle$ is sensitive to the range selected due to the underlying non-QE contribution. The $-0.20 \sim 0.20$ GeV/c momentum range is chosen because it is dominated by the QE events. The results are summarized in Fig. 9.

The average peak positions of MnvGENIE-v1.0.1 lie outside 1σ uncertainty range of the data. Measurable shifts to larger $\langle \delta p_{\mathrm{Ty}} \rangle$ are observed when interaction energy corrections are applied. The shifts are on the order of $15 \sim 20$ MeV/c, consistent with corrections made to the underlying model. The measurements disfavor the default GENIE removal energy implementation, but does not distinguish between the nuclear potential corrections. Among the models NuWro SF, NEUT SF and GiBUU models are comparable to the data average, while NuWro and NEUT LFGs have larger disagreement with the data. Between them, NEUT LFG peaks outside the measurement uncertainties.

Next, we calculate χ^2 distributions in four consecutive, disjoint δp_{Ty} ranges dominated by QE interactions to illustrate the mismodelling in the MnvGENIE-v1.0.1 simulations. Table. IV summarizes the results. The χ^2 in δp_{Ty} for MnvGENIE-v1.0.1 is asymmetric about the 0-axis, where the falling side ($0 \sim 0.2$ GeV/c) is in much better agreement with the data than the rising side ($-0.2 \sim 0.0$ GeV/c). The corrections on MnvGENIE-v1.0.1 turns the asymmetry in χ^2 around, indicating the predicted δp_{Ty} distribution is wider, an effect the removal energy does not account for. The total χ^2 between $-0.2 \sim 0.2$ GeV/c improves significantly after the corrections are applied.

VII. SUMMARY AND OUTLOOK

The variables δp_{Tx} and δp_{Ty} are measured on the CH target in MINERνA. We expect δp_{Tx} to be sensitive to the Fermi momentum in QE and there is tension between data and MC. The data is narrower than the GENIE model, as is true of most models other than a simple Fermi gas. The measurement also shows a statistically marginal proton asymmetry in δp_{Tx} of -0.05 ± 0.02. This asymmetry, if truly non-zero, might be attributed to pion absorption events included in the signal. No model in current event generators predicts an asymmetry. Future measurements could verify the presence of this asymmetry.

The observable δp_{Ty} shows sensitivity to the interac-

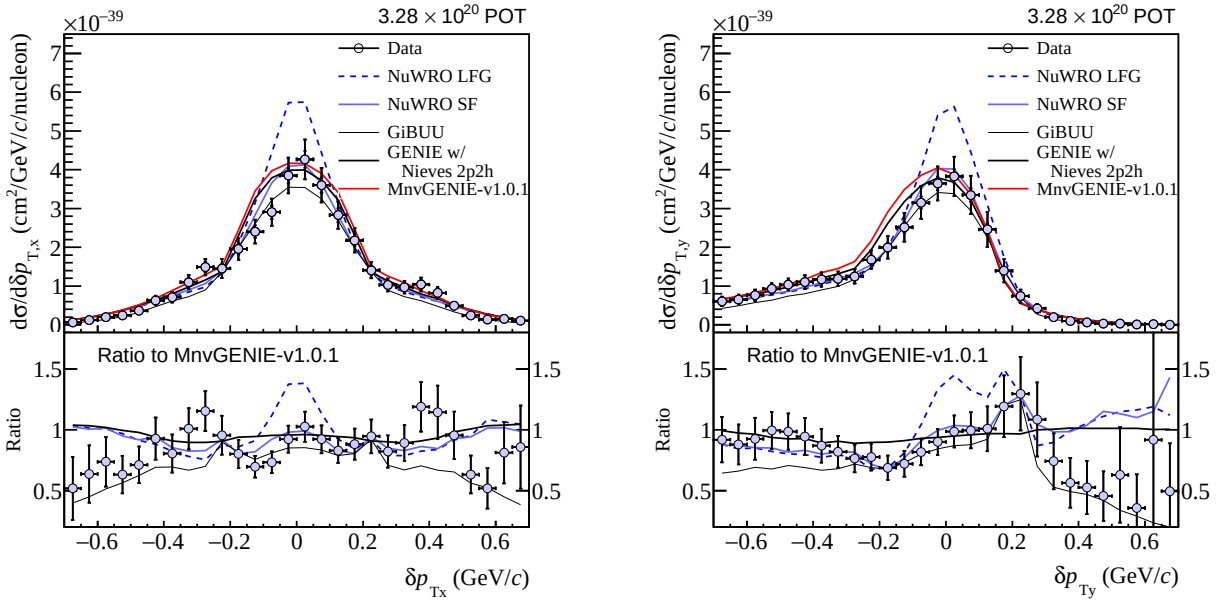

FIG. 7. Model comparisons for NuWro LF, NuWro SF,GiBUU, default GENIE and MnvGENIE-v1.0.1. Both NuWro SF and GiBUUobserve peak shifts consistent with data. NuWro LFG, although more discrepant from the data, describes the narrowness of the data peak well.

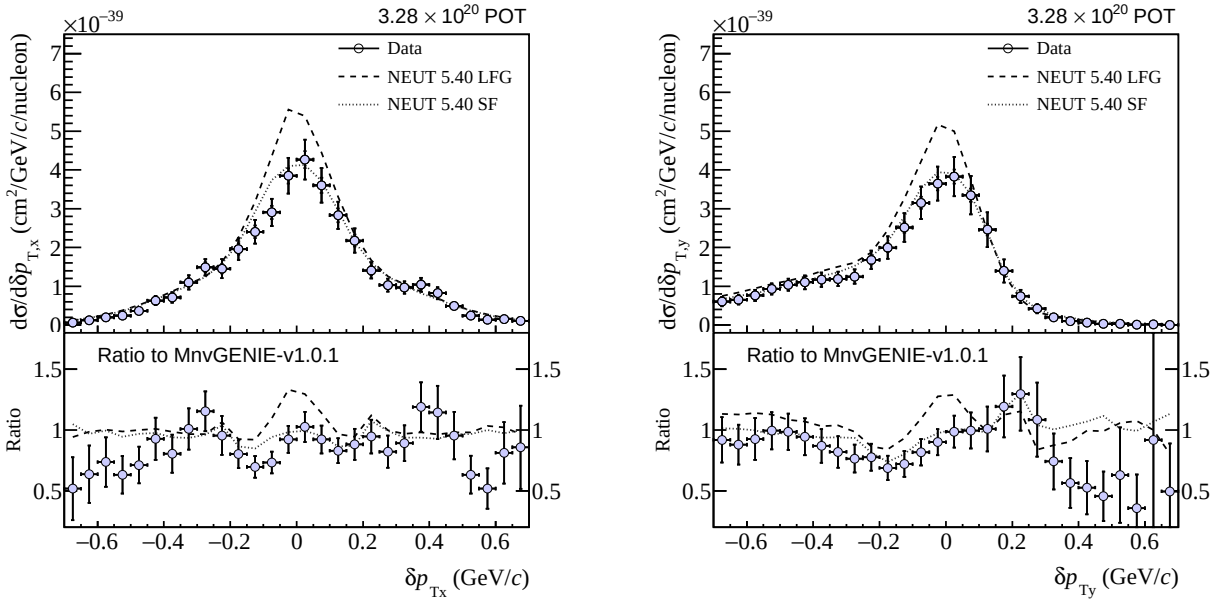

FIG. 8. Model comparisons for NEUT SF and NEUT LFG. The δp_{Ty} distribution in NEUT SF describes the data peak well, while NEUT LFG over-predicts the left side of the peak, leading to a wider peak similar to GENIE.

tion energy implemented in nuclear models. In particular, the measurement, which is based on GENIE, disfavors the default GENIE implementation of the interaction energy on Carbon. This implementation lacks the excitation energy while subtracts an extra Moniz interaction energy from the final state proton. The average peak positions between GENIE and data differ by more than 1.5σ. Approximate corrections accounting for the excitation energy and Moniz interaction energy bring the average peak position within 1σ of the data. This measurement is not precise enough to distinguish the more subtle nuclear effects such as the optical potential and the

TABLE IV. δp_{Ty}: χ^2 comparisons, POT normalized.

POT Normalized	-0.2 ∼ -0.1 GeV	**-0.1 ∼ 0.0 GeV**	**0.0 ∼ 0.1 GeV**	0.1 ∼ 0.2 GeV	-0.2 ∼ 0.2 GeV
MnvGENIE-v1.0.1	59.9/2	**21.9/2**	**1.35/2**	15.5/2	67.9/8
01: U_{opt} only	10.8/2	**5.32/2**	**17.8/2**	38.3/2	21.2/8
02: U_{opt} and V_{eff}	7.2/2	**3.6/2**	**22.8/2**	47.1/2	27.3/8

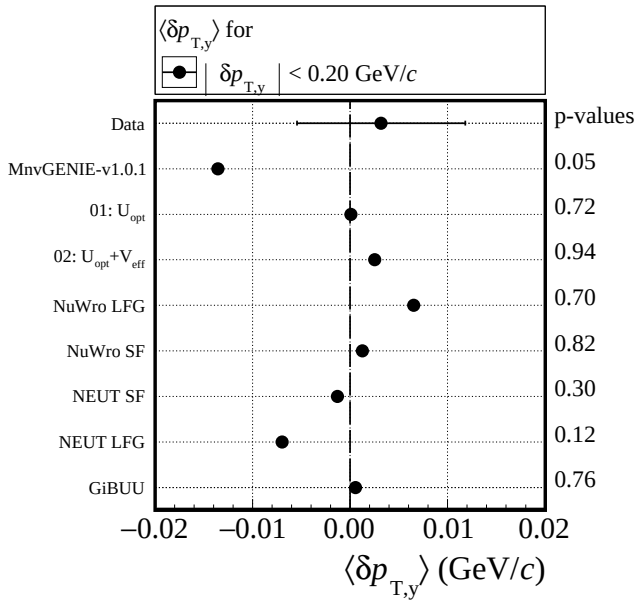

FIG. 9. $\langle \delta p_{\mathrm{Ty}} \rangle$ calculated from the differential cross section within $|\delta p_{\mathrm{Ty}}| < 0.20$ GeV/c. The p-value is the probability, assuming normal distribution, that the observed result would have been produced by change from this model.

Coulomb potential due to the mostly systematics dominated uncertainties.

We have compared different Monte Carlo models with respect to δp_{Tx} and δp_{Ty}. The measurements are based on the MnvGENIE-v1.0.1 tune of GENIE, which removes the elastic FSI components in GENIE on top of the MnvGENIE-v1 base tune. This modification subsequently impact the single-TKI measurements performed in Reference [3]. The elastic FSI is discussed in Appendix B. The Supplemental Material to this paper contains an update to the single-TKI results presented in Reference [3] based on this bug fix.

Future MINERνA analysis with the medium energy beam [36] will benefit from higher statistics and probe the asymmetry in greater detail. Other targets in MINERνA and future liquid argon experiments could make measurements of $(\delta p_{\mathrm{Tx}}, \delta p_{\mathrm{Ty}})$, and the single-TKI variables in general, to test models on other nuclei.

This work was supported by the Fermi National Accelerator Laboratory under US Department of Energy contract No. DE-AC02-07CH11359 which included the MINERνA construction project. Construction support was also granted by the United States National Science Foundation under Award PHY-0619727 and by the University of Rochester. Support for participating scientists was provided by NSF and DOE (USA), by CAPES and CNPq (Brazil), by CoNaCyT (Mexico), by Proyecto Basal FB 0821, CONICYT PIA ACT1413, Fondecyt 3170845 and 11130133 (Chile), by DGI-PUCP and UDI/VRI-IGI-UNI (Peru), by the Latin American Center for Physics (CLAF), by Science and Technology Facilities Council (UK), and by NCN Opus Grant No. 2016/21/B/ST2/01092 (Poland). We thank the MINOS Collaboration for use of its near detector data. We acknowledge the dedicated work of the Fermilab staff responsible for the operation and maintenance of the beam line and detector and the Fermilab Computing Division for support of data processing.

[1] A. Bodek and T. Cai, Eur. Phys. J. **C79**, 293 (2019), arXiv:1801.07975 [nucl-th].
[2] X.-G. Lu, L. Pickering, S. Dolan, G. Barr, D. Coplowe, Y. Uchida, D. Wark, M. O. Wascko, A. Weber, and T. Yuan, Phys. Rev. C **94**, 015503 (2016).
[3] X.-G. Lu *et al.* (MINERνA Collaboration), Phys. Rev. Lett. **121**, 022504 (2018), arXiv:1805.05486 [hep-ex].
[4] K. Abe *et al.* (T2K Collaboration), Phys. Rev. D **98**, 032003 (2018).
[5] C. Andreopoulos (GENIE Collaboration), *Neutrino interactions: From theory to Monte Carlo simulations. Proceedings, 45th Karpacz Winter School in Theoretical Physics, Ladek-Zdroj, Poland, February 2-11, 2009*, Acta Phys. Polon. **B40**, 2461 (2009).
[6] Y. Hayato, *Neutrino interactions: From theory to Monte Carlo simulations. Proceedings, 45th Karpacz Winter School in Theoretical Physics, Ladek-Zdroj, Poland, February 2-11, 2009*, Acta Phys. Polon. **B40**, 2477 (2009).
[7] C. Juszczak, J. A. Nowak, and J. T. Sobczyk, Nuclear Physics B - Proceedings Supplements **159**, 211 (2006), proceedings of the 4th International Workshop on Neutrino-Nucleus Interactions in the Few-GeV Region.
[8] O. Buss, T. Gaitanos, K. Gallmeister, H. van Hees, M. Kaskulov, O. Lalakulich, A. B. Larionov, T. Leitner, J. Weil, and U. Mosel, Phys. Rept. **512**, 1 (2012), arXiv:1106.1344 [hep-ph].
[9] K. Gallmeister, U. Mosel, and J. Weil, Phys. Rev. **C94**, 035502 (2016),

arXiv:1605.09391 [nucl-th].
[10] P. E. Hodgson, Reports on Progress in Physics **34**, 765 (1971).
[11] R. A. Smith and E. J. Moniz, Nucl. Phys. **B43**, 605 (1972), [Erratum: Nucl. Phys.B101,547(1975)].
[12] L. Aliaga *et al.* (MINERνA Collaboration), Nucl. Instrum. Meth. **A743**, 130 (2014), arXiv:1305.5199 [physics.ins-det].
[13] P. Adamson *et al.*, Nucl. Instrum. Meth. **A806**, 279 (2016), arXiv:1507.06690 [physics.acc-ph].
[14] L. Aliaga *et al.* (MINERνA Collaboration), Phys. Rev. **D94**, 092005 (2016), [Addendum: Phys. Rev.D95,no.3,039903(2017)], arXiv:1607.00704 [hep-ex].
[15] X.-G. Lu and M. Betancourt (MINERνA Collaboration), *Proceedings, 27th International Conference on Neutrino Physics and Astrophysics (Neutrino 2016): London, United Kingdom, July 4-9, 2016*, J. Phys. Conf. Ser. **888**, 012120 (2017), arXiv:1608.04655 [hep-ex].
[16] T. Walton *et al.* (MINERνA Collaboration), Phys. Rev. **D91**, 071301 (2015), arXiv:1409.4497 [hep-ex].
[17] G. D'Agostini, Nucl. Instrum. Meth. **A362**, 487 (1995).
[18] A. Bodek and J. L. Ritchie, Phys. Rev. D **23**, 1070 (1981).
[19] C. H. Llewellyn Smith, *Gauge Theories and Neutrino Physics, Jacob, 1978:0175*, Phys. Rept. **3**, 261 (1972).
[20] D. Rein and L. M. Sehgal, Annals of Physics **133**, 79 (1981).
[21] A. Bodek and U. K. Yang, *Proceedings, 1st International Workshop on Neutrino-nucleus interactions in the few GeV region (NuInt 01): Tsukuba, Japan, December 13-16, 2001*, Nucl. Phys. Proc. Suppl. **112**, 70 (2002), [,70(2002)], arXiv:hep-ex/0203009 [hep-ex].
[22] J. Nieves, R. Gran, F. Sanchez, and M. J. Vicente Vacas, in *15th International Workshop on Neutrino Factories, Super Beams and Beta Beams (NuFact2013) Beijing, China, August 19-24, 2013* (2013) arXiv:1310.7091 [hep-ph].
[23] R. Gran, J. Nieves, F. Sanchez, and M. J. V. Vacas, Phys. Rev. D **88**, 113007 (2013).
[24] J. Schwehr, D. Cherdack, and R. Gran, (2016), arXiv:1601.02038 [hep-ph].
[25] P. A. Rodrigues, J. Demgen, E. Miltenberger, *et al.* (MINERνA Collaboration), Phys. Rev. Lett. **116**, 071802 (2016).
[26] C. Wilkinson, P. Rodrigues, S. Cartwright, L. Thompson, and K. McFarland, Phys. Rev. **D90**, 112017 (2014), arXiv:1411.4482 [hep-ex].
[27] P. Rodrigues, C. Wilkinson, and K. McFarland, Eur. Phys. J. **C76**, 474 (2016), arXiv:1601.01888 [hep-ex].
[28] J. Nieves, J. E. Amaro, and M. Valverde, Phys. Rev. **C70**, 055503 (2004), [Erratum: Phys. Rev.C72,019902(2005)], arXiv:nucl-th/0408005 [nucl-th].
[29] R. Gran, (2017), arXiv:1705.02932 [hep-ex].
[30] P. Stowell *et al.*, JINST **12**, P01016 (2017), arXiv:1612.07393 [hep-ex].
[31] T. Cai, X. Lu, and D. Ruterbories, (2019), arXiv:1907.11212 [hep-ex].
[32] G. M. Radecky, V. E. Barnes, D. D. Carmony, A. F. Garfinkel, M. Derrick, E. Fernandez, L. Hyman, G. Levman, D. Koetke, B. Musgrave, P. Schreiner, R. Singer, A. Snyder, S. Toaff, S. J. Barish, A. Engler, R. W. Kraemer, K. Miller, B. J. Stacey, R. Ammar, D. Coppage, D. Day, R. Davis, N. Kwak, and R. Stump, Phys. Rev. D **25**, 1161 (1982).
[33] O. Altinok *et al.* (MINERνA Collaboration), Phys. Rev. D **96**, 072003 (2017).
[34] A. M. Ankowski and J. T. Sobczyk, Phys. Rev. **C77**, 044311 (2008), arXiv:0711.2031 [nucl-th].
[35] T. Leitner and U. Mosel, Phys. Rev. **C81**, 064614 (2010), arXiv:1004.4433 [nucl-th].
[36] P. Adamson *et al.*, Nucl. Instrum. Meth. **A806**, 279 (2016), arXiv:1507.06690 [physics.acc-ph].
[37] L. Harewood and R. Gran, (2019), arXiv:1901.04892 [hep-ex].

Appendix A: Derivations of GENIE corrections

The energy conservation at the vertex in GENIE is

$$\upsilon_{\text{GENIE}} + M_N - S^N - \frac{\langle \mathbf{k}^2 \rangle}{2M_{A-1}^2} = \sqrt{(\mathbf{k}+\mathbf{q}_3)^2 + M_P^2}, \quad \text{(A1)}$$

comparing to Eq.(7), we obtain

$$\upsilon \approx \upsilon_{\text{GENIE}} - |U_{\text{opt}}| + |V_{\text{eff}}^{\text{P}}| + \langle E_x \rangle. \quad \text{(A2)}$$

The difference in energy transfer manifests on the outgoing muon energy:

$$E^\nu - E^\mu = E^\nu - E^\mu_{\text{GENIE}} - |U_{\text{opt}}| + |V_{\text{eff}}^{\text{P}}| + \langle E_x \rangle. \quad \text{(A3)}$$

we obtain the energy correction to the GENIE muon:

$$E^\mu = E^\mu_{\text{GENIE}} + |U_{\text{opt}}| - |V_{\text{eff}}| - \langle E_x^N \rangle \quad \text{(A4)}$$

The outgoing proton energy in GENIE is

$$E^P_{\text{GENIE}} = \sqrt{(\mathbf{k}+\mathbf{q}_3)^2 + M_P^2} - \Delta^{\text{nucleus}}_{\text{GENIE}}. \quad \text{(A5)}$$

Comparing to the right hand side of Eq.(7), we obtain

$$E^P = E^P_{\text{GENIE}} + \Delta^{\text{nucleus}}_{\text{GENIE}} - |U_{\text{opt}}| + |V_{\text{eff}}^{\text{P}}|. \quad \text{(A6)}$$

These corrections largely conserve energy, the effect of E_x on the proton momentum is small; however, momentum conservation would also require corrections to the outgoing particle directions, which are ignored [1].

Appendix B: GENIE elastic FSI simulation

This section will discuss the elastic FSI prediction and fixes to it in more detail.

The prediction from MnvGENIE-v1 in δp_{Tx} has three distinct regions shown in Fig. 10: a non-CCQE tail

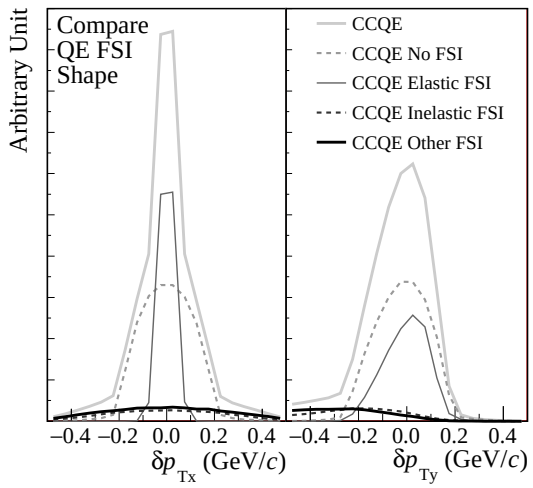

FIG. 10. GENIE FSI modes breakdown for CCQE events. The non-interacting fraction is symmetric and preserves the Bodek-Ritchie Distribution while the GENIE elastic FSI appears accelerated with respect to the transverse momentum transfer q_T.

beyond $|\delta p_{\mathrm{Tx}}| \gtrsim 0.2$ GeV/c, a no FSI CCQE dominated region in $0.2 \gtrsim |\delta p_{\mathrm{Tx}}| \gtrsim 0.1$ GeV/c, which reflects the Fermi momentum, and an elastic FSI peak at $|\delta p_{\mathrm{Tx}}| \lesssim 0.1$ GeV/c. The GENIE elastic FSI is sharply peaked and much narrower than the underlying Fermi gas distribution. Since the protons in the elastic FSI peak followed the no FSI distribution before the FSI simulation, we expect the width of the elastic FSI distribution to be at least as large as that of the no FSI distribution.

Hints of the unphysical nature of the angular distribution already appeared in the original single-TKI analysis reported in Reference [3]. MINERνA uses the default GENIE configuration of version 2.12 which uses the "hA" model for FSI. In this model, every nucleon experiences exactly one of the following fates: 1) no FSI, 2) charge exchange with single nucleon knockout, 3) elastic hadron+nucleus scattering, 4) inelastic single nucleon knockout, 5) multi-nucleon knockout (including pion absorption) and 8) pion production. An advantage of this model is that a reweighting technique can be used to modify the relative mix of fates without fully regenerating Monte Carlo samples. This is convenient for studying FSI systematic effects with an analysis, similar to the existing FSI uncertainties available with the GENIE hA model.

The routine used to calculate all FSI reactions involving a two body scatter contains (in GENIE versions 2.6 to version 3.0.6) a mistake that affects hA fates "2" and "4" (nucleon knockout, with and without charge exchange) and fate "3" (elastic hadron nucleus scattering) for both protons and pions. Fate "3", combined with quasielastic events and single-TKI variables, create the largest in observable distributions. The error in the code results from calculating the boost and scattering in a way that mixes lab frame information when doing the center of momentum scattering calculation.

The primary effect is on the angular distribution of the scattered hadrons. In the QE case the original code causes too few of the most highly-transverse protons, which have low efficiency to be tracked in the MINERνA planar design. It also produces a population, especially of QE events, with a very narrow angle distribution, and in quantities derived from those angular distributions, like many of the single-TKI observables. The angular distribution relative to the lepton and other hadrons are separately affected. This combination affects the predicted distributions presented in Reference [3] in multiple ways. In addition, the resulting hadrons pick up an acceleration of up to 2 MeV. This is smaller than most hadronic energy uncertainties and has negligible role in selection or calorimetry. Instead it appears as an unphysical population in all single-TKI populations in Reference [3]. The largest effects of the distorted input model, after performing the iterative unfolding procedure, are on the acceleration angle and the coplanarity angle.

The study reported in Reference [37] suggests reweighting up the no FSI fate and removing the elastic fate contributions will sufficiently mimic the proton distributions in a fixed code without having to regenerate all MC. Figure 11 shows the effect of fixing the GENIE code and comparing key QE proton distributions. The reason is that the intended elastic scattering angle for protons and neutrons is always small: 90% would be less than 8°. For this analysis, the weights are only applied to GENIE quasielastic events; the distortion of angles for non-quasielastic events with multiple hadrons has a small effect on these distributions.

Among other modifications to FSI, GENIE v3 also removes the elastic FSI component (but not yet fixing the code for other two-body fates). In these new versions the event rate is replaced with nucleons and pions that undergo the other FSI fates rather than events that do not have a FSI. Though not available for analysis at this time, this may result in a significantly different prediction for MINERνA's single-TKI cross sections.

Figure 12 shows the shifts in the data and MC prediction after the reweights have been applied. The 2σ shift in the first data point is the largest of all the shifts in the cross section. All model distributions are modified significantly, but the extracted cross section shifts are only significant in some bins of $\delta\phi_{\mathrm{T}}$ and $\delta\alpha_{\mathrm{T}}$.

The Supplemental Material to this paper contains an update to the single-TKI results presented in Reference [3] based on this bug fix.

Citation of the new cross sections should include this paper and the original paper [3] describing the full methmod.

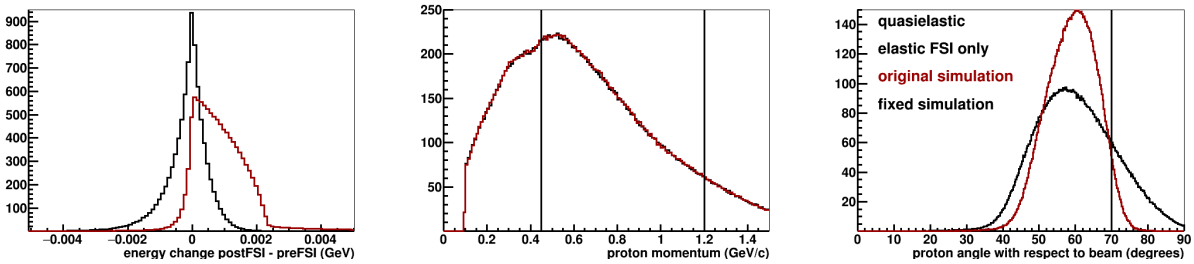

FIG. 11. Comparison of the effect of fixing the GENIE code and comparing key QE proton distributions. Left: Proton acceleration showing the old code produced less than 2 MeV shift. Middle: the small energy shift has negligible effect on the momentum distribution. Right: a major distortion of the angle distribution is what affects the single-TKI analyses; the correct angle distribution is similar to protons (not shown) which had no FSI. Before the fix, this and other distributions based on proton angle such as Fig. 10 are too narrowly peaked. [37]

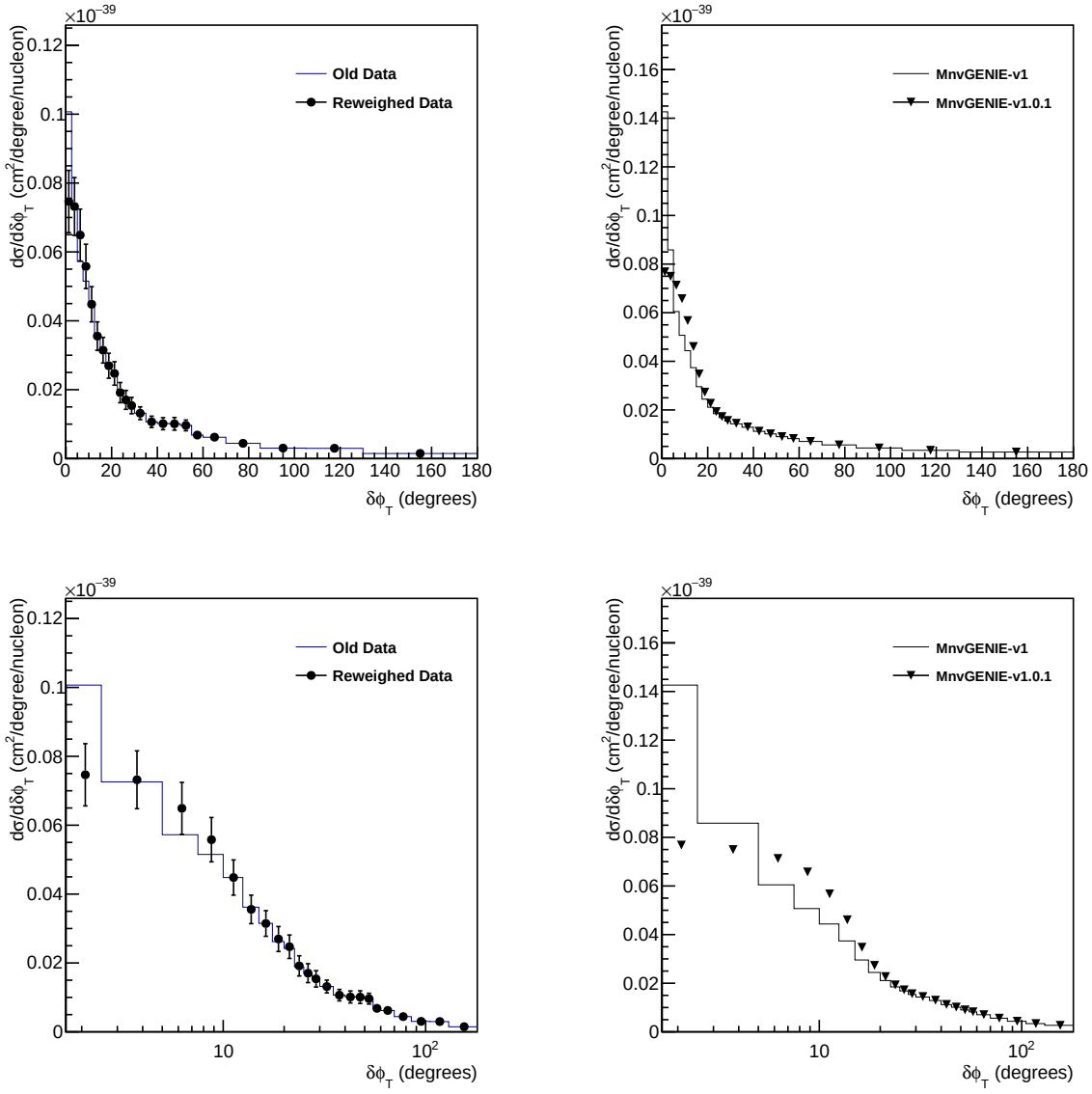

FIG. 12. $\delta\phi_{\mathrm{T}}$ is the angular projection of proton transverse momentum. The original FSI code produces a peak at $0(rad)$ indicating protons were being produced in the reaction plane more often than Fermi-motion would give. The first cross section data point is the only one that shifted by more than 2σ.